Scanning Electrochemical Microscopy: A Multiplexing Tool for Electrochemical DNA Biosensing

33

Mohtashim Hassan Shamsi and Heinz-Bernhard Kraatz

Contents

Introduction 1074
History of SECM 1074
Principle of Feedback Mode of SECM 1075
Approach Curve and Tip Geometry 1077
DNA Films and Self-Assembled Monolayers (SAMs) on Gold Surface 1079
Multiplexed DNA Visualization of Hybridization and Mismatch Detection 1081
Conclusion 1088
References 1092

Abstract

Scanning electrochemical microscopy (SECM) translates the current generated by an electrochemical reaction occurring at a tip electrode scanned across a surface substrate into an image. SECM not only provides a simple electrochemical image of the conductive and/or insulating substrate but also provides kinetic information of the heterogeneous electron transfer reactions when the tip electrode approaches the surface. Applications including biosensing have been demonstrated. In this chapter, we will focus on recent advances in the application of SECM toward the label-free detection of base pair mismatches in DNA.

Despite having nanometer dimensions, the base pair mismatches along a DNA strand can be readily detected by SECM in an array format through exploiting the negative charge in the vicinity of self-assembled DNA films. The response can be amplified using metal ions to enhance the discrimination

M.H. Shamsi • H.-B. Kraatz (✉)
Department of Physical and Environmental Sciences, University of Toronto Scarborough, Toronto, ON, Canada

Department of Chemistry, University of Toronto, Toronto, ON, Canada
e-mail: bernie.kraatz@utoronto.ca

M. Aliofkhazraei, A.S.H. Makhlouf (eds.), *Handbook of Nanoelectrochemistry*,
DOI 10.1007/978-3-319-15266-0_35

between matched and mismatched DNA films. This simple strategy has been used to probe the position of a single nucleotide mismatch, the type of the mismatch, and hybridization position of complementary strand and even allows the identification of various animal species.

Keywords
Scanning electrochemical microscopy • Impedance spectroscopy • DNA • Mismatch • Surfaces • Biosensor

Introduction

Scanning electrochemical microscopy (SECM) is a surface probe microscopic (SPM) tool to study surfaces by electrochemical profiling of surfaces at submicron-level resolution. Electrochemical profiling is monitoring an electrochemical reaction between a biased tip and substrate in contrast to monitoring force in atomic force microscopy and tunneling current in scanning tunneling microscopy. SECM has been widely employed to study nonbiological and biological systems in research areas ranging from corrosion science, catalysis and fuel cells, self-assembled monolayers, polymer coatings, transport through membranes and biological tissue, enzymatic reactions, high-throughput DNA biosensing, studying cell metabolism, and monitoring immiscible interfaces such as gas/liquid interface. SECM also has potential to be coupled with other analytical techniques such as surface plasmon resonance [1] and atomic force microscopy [2]. This present chapter will provide a brief overview of the principles and feedback modes of SECM operation followed by a discussion of label-free DNA hybridization and mismatch detection by SECM. There are a number of excellent reviews available that cover the theory of SECM [3, 4]and its application to the study of biophysical and bioanalytical systems [5, 6], including the study of living cells and their metabolism [7].

History of SECM

In 1986, the fundamental experiments by Engstrom et al. [8] and Liu et al. [9] on using microelectrodes to probe diffusion layers and studying electrode surfaces by scanning electrochemical and tunneling ultramicroelectrode microscope in solution laid the foundation of scanning electrochemical microscopy. In 1989, Kwak and Bard [10] framed a quantitative detail of the diffusion-limited current at a UME as a function of the distance d above a macroscopic planar substrate providing a theoretical description of (a) how the Faradaic current measured at the tip can be a function of charge transfer properties of substrate, (b) the relationship between the Faradaic current obtained at the tip and the tip-substrate distance, and (c) the relationship between diffusion and homogeneous reaction kinetics in the gap between tip and substrate.

SECM imaging is carried out either in generation-collection mode (GC) or in feedback mode (FB). Because of the extensive use of feedback mode to study self-assembled DNA films, we will focus on the principle and theory of FB mode here.

Principle of Feedback Mode of SECM

Typically, a three-electrode assembly, consisting of a working, a counter, and a reference electrode, is used (Fig. 1a) in which a biased ultramicroelectrode tip approaches a substrate in presence of a redox-active mediator. The substrate can be conductive or insulating. The current is generated by a diffusion-limited redox reaction at the tip, i.e., $R \rightarrow O + ne^-$, thus generating a current. The current for a disk electrode can be given as

$$i_\infty = 4nFDC^o a \tag{1}$$

where n = number of electrons/redox couple, F = Faraday constant, D = diffusion coefficient of redox couple, C^o = concentration of redox mediator, a = radius of the disk electrode. The tip current (i_T) follows the relationship when away from substrate. When the tip approaches the substrate in micrometer steps using a piezoelectric positioner, the diffusion-limited tip current (i_T) either rises or falls, depending on the charge transfer property of the substrate as shown in Fig. 1b–d. If the substrate is insulating or electrochemically inert, the diffusion of the redox mediator to the tip from bulk solution is physically hindered, causing a decrease of the current, i.e., $i_T < i_\infty$. If the substrate is conducting, the rate of reaction Eq. 1 can be controlled by applying a suitable potential to the substrate. Otherwise, the potential of a conductive substrate E_s may be determined by the concentration of redox species in solution without an external bias. For example, if the solution contains only the reduced form of the redox species, most of the substrate surface, which is usually much larger than that of the tip, is exposed to solution of R. According to the Nernst equation

$$E_s = E^0 + \mathrm{RT}/\mathrm{nFln}\left(C_o / C_r\right) \tag{2}$$

considering, $C_o \sim 0$, and $E_s - E^0 << 0$, where E^0 = redox mediator standard potential, thus all oxidized species reaching the substrate get reduced at the surface.

Since regeneration is faster at the distance almost equal to the radius of the tip, between the tip and substrate, it causes a sharp increase in the current, i.e., $i_T > i_\infty$. This mode of SECM is called "feedback mode" where a positive feedback ($i_T > i_\infty$) is observed on conducting surfaces and a negative feedback ($i_T < i_\infty$) is observed on insulating surfaces. The rate of heterogeneous electron transfer on the tip electrode is the main parameter that can be extracted from these measurements. There may be one of three ways to regenerate a mediator, i.e., (a) electrochemical conversion of the mediator at the substrate, (b) an enzyme-catalyzed reaction with consumption of O and regeneration of R, or (c) local oxidation of the substrate by O.

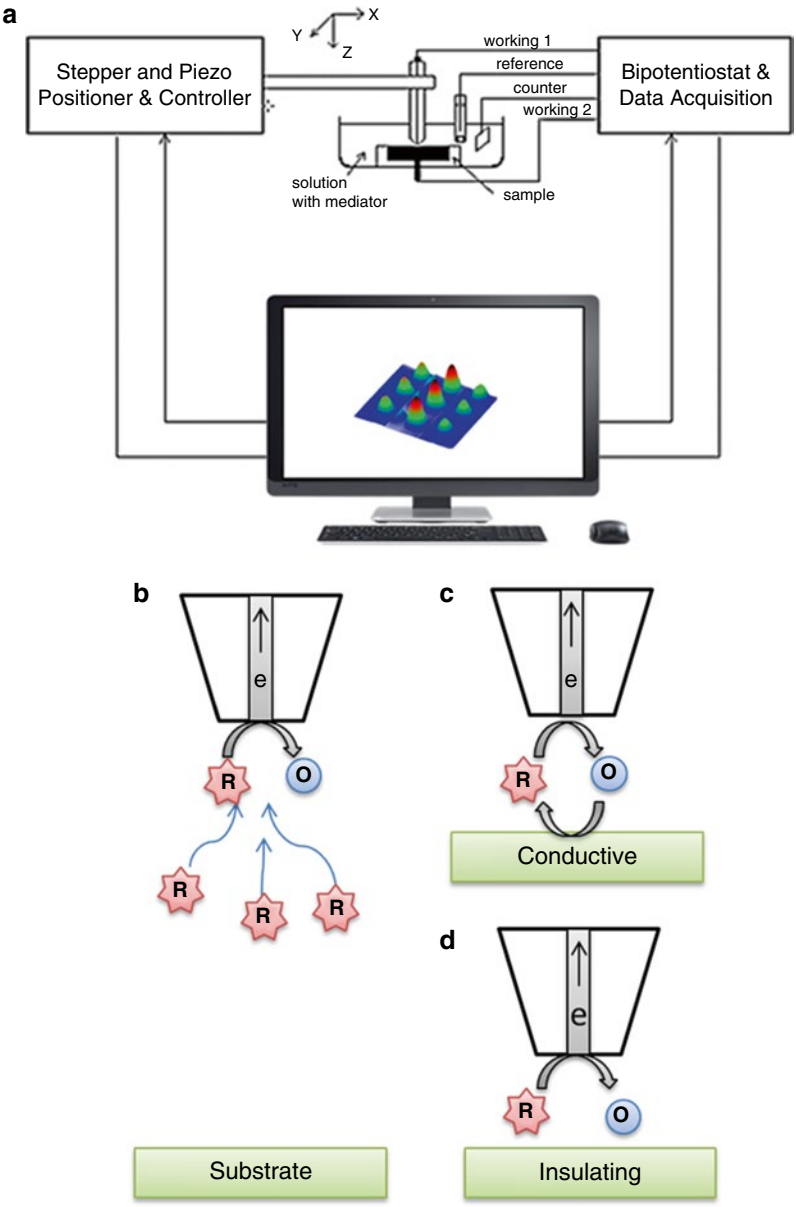

Fig. 1 (**a**) Block diagram of SECM cell connected to a stepper and piezoelectric controller and bipotentiostat. Piezoelectric positioning and applied potential can be controlled through software in PC. (**b**) SECM tip away from substrate in redox mediator solution. When a positive potential is applied, a reducing agent in solution diffuse to the UME tip and get oxidized. (**c**) When UME tip approaches close to a conductive substrate, the oxidized redox mediator is regenerated at the surface of substrate resulting in positive feedback. (**d**) When UME tip approaches close to a insulating substrate, the diffusion of the redox mediator is hindered due to a very small distance between the tip and substrate as well as oxidized redox mediator is not regenerated at the surface of substrate resulting in negative feedback

Approach Curve and Tip Geometry

When the tip is laterally – from the z-direction – brought to the surface with high accuracy of submicron steps, i_T is recorded versus lateral distance d and plotted as "approach curves" (Fig. 2a). The approach curves represent the normalized current $I_T = i_T/i_{T,\infty}$ as a function of the normalized distance $L = d/a$, where d is the distance in z-direction and a is the radius of disk electrode. The normalized approach curves are independent of the mediator concentration C^o, the diffusion coefficient D, and the tip radius a. The normalized tip current I_T depends only on L and the thickness of the insulating sheath forming thin-layer cell with the substrate. Simulations accounting for the amperometric response due to diffusion of the redox species around the corner of the insulating sheath for a wide range of tip-substrate distances over conducting and insulating substrates were performed for several RG ratios [11]. Diffusion around the edge of the insulating sheath was found to have a pronounced effect on the approach curves. The tip currents for conducting substrates were found significantly dependent on the tip geometry. The resolution of the image largely depends on the geometry and size of the ultramicroelectrode probe tip. Sharper tips (i.e., lower RG) produce a high-resolution image and a high feedback current. SECM also provides quantitative information about the electrochemical properties

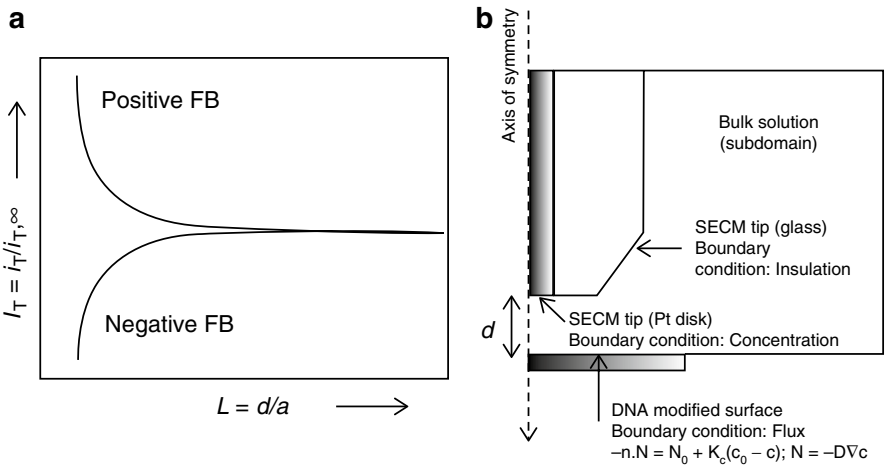

Fig. 2 (**a**) Approach curves (normalized tip current vs. normalized distance) recorded over the conductive substrate giving positive feedback current and an insulating substrate giving negative feedback current. (**b**) Sketch of numerical simulation to extract the reaction kinetics between the tip and substrate. Here, the steady-state diffusion problem for SECM geometry was solved numerically assuming irreversible substrate kinetics, in dimensionless form using the finite element method (COMSOL Multiphysics 3.5a software with Chemical Engineering Module) (Figure 2b has been taken from Diakowski P, Kraatz H-B (2011) Towards the electrochemical identification of species. Chem Comm 47:1431–1433 with permission from The Royal Society of Chemistry)

of a surface through numerical modeling. The simulations are useful to assess the SECM topographical sensitivity, i.e., the rate of change of tip current with respect to tip-substrate distance, and spatial resolution, i.e., the ability of the microdisk electrode to distinguish two conducting islands embedded in an insulating substrate. A system under investigation can be numerically modeled using the dimensions of the tip electrode, substrate, and the inter tip-substrate distance, which provides kinetics of the reaction under observation by simulations as shown in Fig. 2b. Theoretical approach curves can be obtained by setting the boundaries and varying d in numerical simulation. Recently, COMSOL Multiphysics 3.5a software with Chemical Engineering Module has been used to solve steady-state diffusion problems for SECM geometry by assuming irreversible substrate kinetics and using the finite element method in dimensionless form [12, 13].

Numerical simulation allowed the calculation of theoretical approach curves for different values of a dimensionless rate constant, Λ, which can be described as

$$\Lambda = k^0 a / D \tag{3}$$

where k^0 = apparent rate constant, a = radius of the tip, and D = diffusion coefficient of the redox mediator. In this case, the apparent rate constant accounts for the combined contributions of electron transfer across the film and penetration of the redox mediator into the film [14]. The diffusion coefficient for the redox mediator can be obtained from Eq. 1 $i_\infty = 4nFDC^o a$. Experimental data modeled on the above method allows evaluation of the apparent rate constants for electron transfer across DNA films.

The tips in the range 5–25 μm have been widely used for biophysical application along with the development toward submicron probes to study smallest possible areas with high resolution. Traditionally, the SECM tip is prepared by heat sealing of a metal wire having diameter in micron scale in a glass capillary under vacuum (Fig. 3) followed by connection with external copper wire using silver epoxy on the other side of the capillary. The size of the glass sheath surrounding the disk electrode is reduced through manual polishing with rotating polishing pads using 3.0 and 0.05 μm alumina particles to minimize the electrode RG. The obtained tip electrodes can be evaluated under microscope and tested electrochemically by performing cyclic voltammetry and SECM approach curves on conducting or insulating surfaces. Following procedures carefully may allow obtaining tip electrodes with RG value between 2 and 3. Nanometer- and submicron-sized tips can also be produced for the application of SECM-AFM by chemical etching of a metal wire followed by insulator coating leaving the apex exposed. Mirkin and coworkers studied the kinetics of fast heterogeneous ET reactions using flat Au nanoelectrodes by SECM [15]. The rate of mass transfer by diffusion was varied by changing the tip radius (a) and the tip-substrate distance (d); the kinetic parameters were found to be independent of both a and d. The reaction kinetics were found dependent on electrode material for some electroactive species, such as $[Ru(NH_3)_6]^{3+}$, and independent of electrode material for species such as ferrocene or ferrocenemethanol when compared to Pt nanoelectrodes [15].

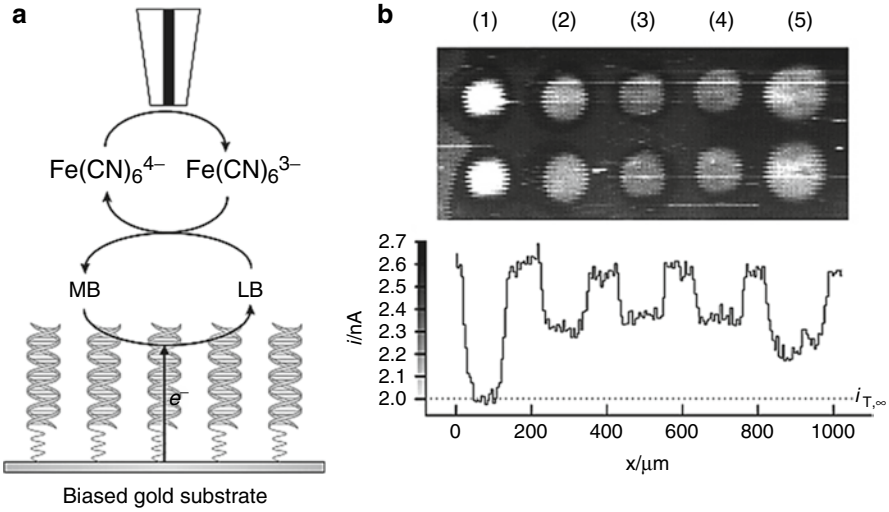

Fig. 3 (**a**) Schematic depicting the catalytic electron transfer between the biased gold substrate to the tip electrode through self-assembled DNA film via intercalated methylene blue and solution based ferro/ferricyanide. MB is reduced by the electron transfer from the biased gold substrate and then regenerated by donating electron to ferrocyanide which is reoxidized to ferricyanide on the tip electrode. (**b**) Multiplexed SECM image and current profiles of a DNA microarray immobilized on a gold disk substrate biased at −0.4 V containing 2 mM $K_4Fe(CN)_6$ and 2 μM MB. Both rows of spots correspond to (*1*) ss-DNA, (*2*) complementary ds-DNA, (*3*) one base mismatch ds-DNA, (*4*) two base mismatches ds-DNA, and (*5*) three base mismatches ds-DNA (Reprinted with permission from Wain A, Zhou F *Langmuir* 24:5155–5160. Copyright (2008) American Chemical Society)

DNA Films and Self-Assembled Monolayers (SAMs) on Gold Surface

After providing a brief introduction to SECM, we next want to redirect the discussion to the application of SECM for the study of thin films composed of deoxyribonucleic acid (DNA). DNA is a biological polymer composed of nucleotide monomeric blocks, which are linked through a phosphodiester linkage. There are two purine bases, adenine (A) and guanine (G), and two pyrimidine bases, thymine (T) and cytosine (C), which pair up in the Watson-Crick sense as A-T and G-C pairs, resulting in the formation of two antiparallel strands of DNA. Deoxyribonucleic acid has three different conformations, A, B, and Z. Under physiological conditions, the most common conformational form is B-DNA, which is a right-handed helix with a diameter of approximately 2.0 nm, a pitch of 10.5 base pairs (bp), and a separation of 0.34 nm between two successive bases. The separation of the sugar-phosphate backbone of the two antiparallel strands due to base pair stacks and repulsion between anionic phosphate groups give rise to a pair of grooves, the minor

and major grooves, that runs along the length of the duplex. These grooves facilitate base access for molecular recognition events. When DNA strands are immobilized on gold surfaces through Au-S linkages, the footprint area occupied by a ds-DNA strand on surface is about 3.14 nm^2, neglecting the hydrodynamic volume, while the length for a 30 base pair construct of ds-DNA is ~10.2 nm. A surface-immobilized single-stranded or double-stranded DNA not only physically passivates the surface but also makes the surface negatively charged due to poor shielding of the backbone charge by monovalent cations. The presence of base pair mismatches in ds-DNA can create significant distortions in the backbone structure. The presence of a mismatch destabilizes a duplex relatively by 1.7–10.0 kcal/mol depending upon position and type of mismatch as well as concentration of Na^+ ions [16], consequently lowering the melting temperature T_m [17]. The important parameters of different conformers of double-stranded DNA are given in Table 1.

Self-assembly of DNA on gold surfaces is similar to organic self-assembled monolayers (SAMs), therefore it seems appropriate to discuss SAM behavior briefly in the light of SECM. Please note that DNA films lack the organization that is characteristic to alkythiols including the tight packing of molecules. Organic SAMs have been extensively studied by SECM. Steady-state measurements by SECM eliminate problems associated with double-layer charging as well as contributions due to oxide film formation and reduction. The small size of the tip and currents minimizes problems of *iR* drop and allows fast mass transport to occur, which is good for monitoring fast reactions [18]. Patterned SAMs on gold have been imaged through the local inhibition of electron transfer [19–21]. A well-packed nonconductive SAM covers the gold substrate and behaves like an insulator. Possible defects in the monolayer can be readily detected by SECM due to a lower i_T in the SAM-modified gold region and high i_T in the loosely packed areas or bare gold region. A sharper tip, having a lower RG, provides high-resolution details by providing a good contrast between SAM-covered areas and bare gold surfaces thus detecting

Table 1 Parameters of common conformers of double stranded DNA

Properties	Z-DNA	B-DNA	A-DNA
Helical turn	Left-handed	Right-handed	Right-handed
Length/residue (Å)	3.7	3.4	2.55
Pitch (residue/turn)	11.6	10.5	11
Rotation/residue	–60°/2 bp	36.0°	32.7°
Inclination of basepair towards axis	0.1°	2.8°	22.6°
Diameter (Å)		20	
Foot print area (Å)		314	
Destabilization due to single mismatch (kcal/mol)		1.7–10.0	

Parameter values adopted from P. Belmont, J.-F. Constant, M. Demeunynck, Chem. Soc. Rev. 30, 70 (2001); S. Neidle, Nucleic Acid Structure and Recognition, Oxford University Press, New York, 2002

the defects on the SAM-covered areas. The quality of the SAM can be evaluated by following the reaction kinetics using approach curves. SECM can differentiate the properties of terminally functionalized SAMs as a function of different chain length, amount of protonation, or complex formation [22, 23]. SAMs can be neutral or charged depending on the end groups, therefore a thoughtful selection of the redox mediator is required to address a specific question since if the SAM is negatively charged, then use of positively charged redox mediator will give an opposite response on measuring current in contrast to negatively charged redox mediator.

Multiplexed DNA Visualization of Hybridization and Mismatch Detection

Yamashita et al. [24] first time visualized DNA duplexes, poorly though, on gold surface in microarray format (DNA spot ~300 μm) by SECM in the electrolyte containing the intercalator ferrocenylnaphthalene diimide as a hybridization indicator. The idea was to discriminate ds-DNA containing base pair mismatches from a matched ds-DNA monitoring the difference in the amounts of intercalation between matched and mismatched duplexes. The study did not provide any quantitative information or clear discrimination between matched and mismatched ds-DNA.

Zhou and coworker [25] demonstrated the DNA hybridization detection by staining the DNA spots with silver particles. The higher feedback current due to regeneration of $[Ru(NH_3)_6]^{3+}$redox mediator by silver particles confirmed the hybridization event. They claimed achieving detection limit of 30 mol of target per spot, however with poor imaging and significantly large microarray format ~ 500 μm size/spot. They also demonstrated the DNA hybridization detection through tip-induced oxidation of guanine residues in the DNA molecules by generating $[Ru(bpy)_3]^{2+}$at the tip electrode. Imaging of DNA hybridization via guanine oxidation is a label-free approach. However, its oxidation is a destructive approach to discriminate between guanine-rich and guanine-poor DNA [26]. This strategy may not be an attractive way of detection for the samples lacking guanine bases. Subsequent studies employed methylene blue (MB) as a redox-active DNA intercalator and ferrocyanide as redox mediator in solution to image DNA microarrays fabricated on gold substrates (Fig. 4) [27]. The labeled approach involved catalytic regeneration of intercalated MB, by tip-generated ferricyanide, which was electrochemically reduced by electron transfer from the gold substrate. Subsequently, the feedback current is used to extract the heterogeneous electron transfer rate constant for the MB-intercalated DNA. In this work, they were able to discriminate between single-stranded and double-stranded oligomers as well as mismatched ds-DNA.

In contrast to Zhou and coworkers' insight of electron transfer through DNA film, there is another view, which involves electron transfer through the DNA π-stack from substrate to tip. It was postulated that the electrocatalytic cycle involving the oxidation of leucomethylene blue (LB) by tip-generated $[Fe(CN)_6]^{3-}$ proceeds via long-range heterogeneous electron transfer mediated by the DNA π-stack.

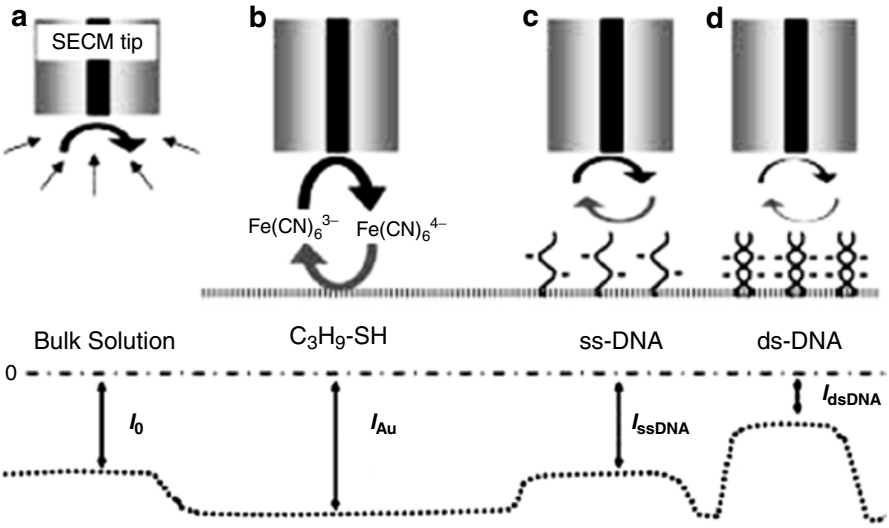

Fig. 4 Scheme depecting repelling-mode SECM. (**a**) A diffusion-limited steady state reduction current is recorded in $[Fe(CN)_6]^{3-}$ solution at 0 mV (vs. Ag/AgCl) tip potential. (**b**) Recycling of tip-generated $[Fe(CN)_6]^{4-}$ to $[Fe(CN)_6]^{3-}$ occurs with the SECM tip close to a propane thiol-modified gold surface resulting in increase in tip current because of positive feedback redox cycling. (**c**) Above a ss-DNA, tip-generated $[Fe(CN)_6]^{4-}$ experience charge repulsion with the oligonucleotide backbone causing a hindrance in diffusion of the mediator to the gold surface, thus modulating the diffusion rate which decreases tip current. (**d**) Hybridization increases the density of anionic phosphate groups leading to a further drop in tip current owing to enhanced repulsion of the redox mediator molecules (Extracted from Turcu F, Schulte A, Hartwich G, Schuhmann W *Angew. Chemie* (*Int. Ed.* in English) 43:3482–3485. John Wiley & Sons, Inc. (2004))

Disruptions in the DNA π-stack due to a single-base mismatch or a basic site disrupts the electrochemical catalytic cycle [28]. A similar approach was used in a study reported by Gorodetsky et al [29] to probe long-range charge transfer through the π-stack of DNA film containing the redox-active intercalator Nile blue (NB) covalently attached at discrete sites along the individual DNA helices. NB attached close to the solution side of the film is involved in the catalytic regeneration of ferrocyanide present in solution. It is important to note here that there is conflicting data, which will undoubtedly require further investigation of a possible DNA-mediated charge transfer between redox probes and the electrode surface. The impact of small defects in the SAMs as well as possible electronic conduction by hopping between differently located intercalated redox species by intra- and interstrand exchange need to be investigated. Since the biopolymer films are usually constructed of dense monolayers, one may query as how hopping and tunneling mechanisms would work, even though the redox signals measured are within a potential range where DNA bases are neither reduced nor oxidized [30].

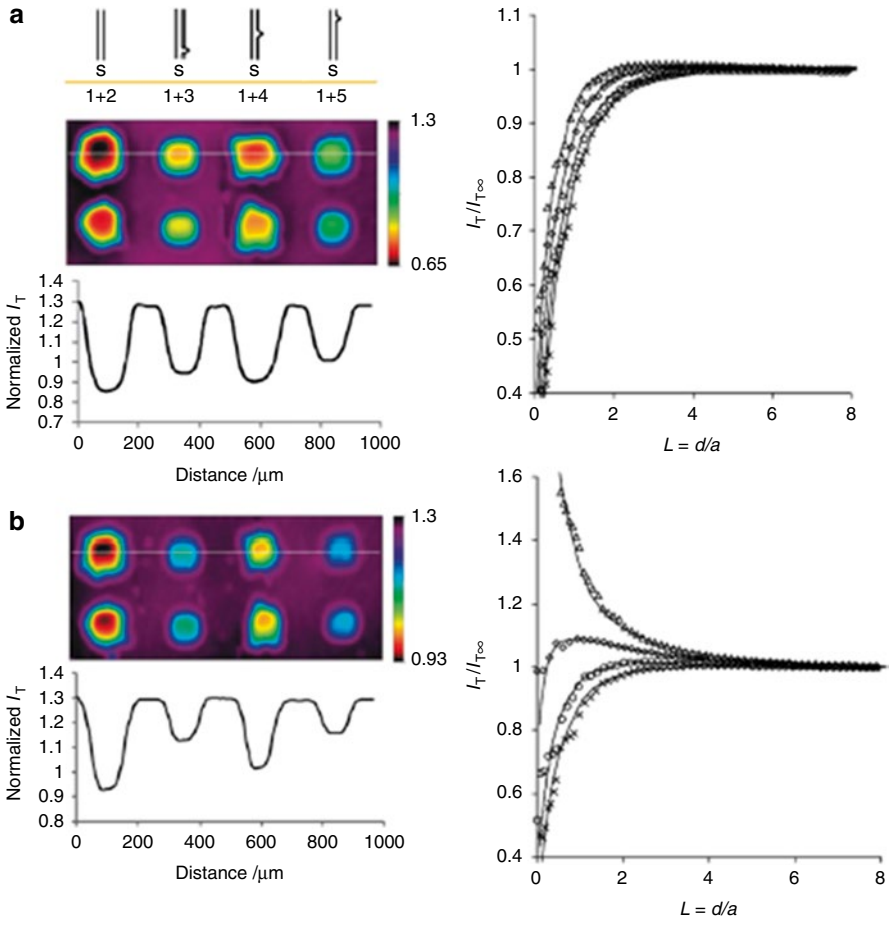

Fig. 5 Multiplexed charge repelling mode SECM images, current profiles and approach curves of ds-DNA microarrays in absence (**a**) and presence (**b**) of Zn^{2+}. 1 + 2 = fully matched, 1 + 3 = bottom mismatch, 1+ 4 = middle mismatch and 1 + 5 = top mismatch duplexes (Figure adapted from Diakowski P, Kraatz H-B (2009) Detection of single-nucleotide mismatches using scanning electrochemical microscopy. Chem Comm 45:1189–1191 with permission from The Royal Society of Chemistry)

Turcu et al. [31] introduced an electrostatic approach, exploiting charge repulsion, to visualize the surface-bound DNA hybridization process. The approach involves exploiting the Coulombic interactions between a negatively charged solution-based redox mediator, $[Fe(CN)_6]^{4-}$, and the backbone phosphodiester groups of the immobilized DNA strands as shown in Fig. 5. Electrostatic repulsion between phosphate groups of DNA and ferricyanide controls the diffusion transport properties of the dissolved mediator to the gold surface at DNA-modified regions. The increase in the density of the negative charge due to hybridization makes electrostatic repulsion a sensitive method to visualize hybridization. The effects of different factors including

probe and mediator concentrations, ionic strength, and tip-to-sample distance were studied in a separate study [32]. The feedback mode is particularly versatile in detecting hybridization events by exploiting biocatalytic reactions [33], signal amplification through enzymatic reaction by labeling capture or target strand [34, 35], and detecting surface-adsorbed matched and mismatched genomic DNA in a microarray format on polymer-coated carbon screen-printed electrodes [36].

Using the charge-repelling mode, Liu et al. [37] calculated the rate of electron transfer across self-assembled DNA duplexes on gold surfaces in absence and presence of Zn^{2+}. In absence of Zn^{2+}, the apparent rate constant for heterogeneous electron transfer from a dissolved redox probe, $[Fe(CN)_6]^{3-/4-}$, to the gold surface through ds-DNA was ~4.6×10^{-7} cm s^{-1}, which increased to ~5.0×10^{-6} cm s^{-1} in presence of the metal ion. The increase in rate constant was also observed with noncomplexing Ca^{2+} and Mg^{2+} ions, which inferred that the binding of these cations facilitated the penetration of DNA film by the negative probe mediator, thereby resulting in an increased redox signal. In contrast, cationic and neutral mediators were found to be unaffected by the ds-DNA film. In a combined SECM and impedance spectroscopy study in the presence of Zn^{2+} [38], Kraatz and coworkers addressed several interesting and legitimate questions in the area of DNA hybridization and mismatch detection. Diakowski and Kraatz [39] demonstrated that repelling-mode SECM can detect the presence and position of A-C single-nucleotide mismatches in unlabeled ds-DNA films, by monitoring change in the amperometric feedback current in the absence and presence of Zn^{2+} (Fig. 6).

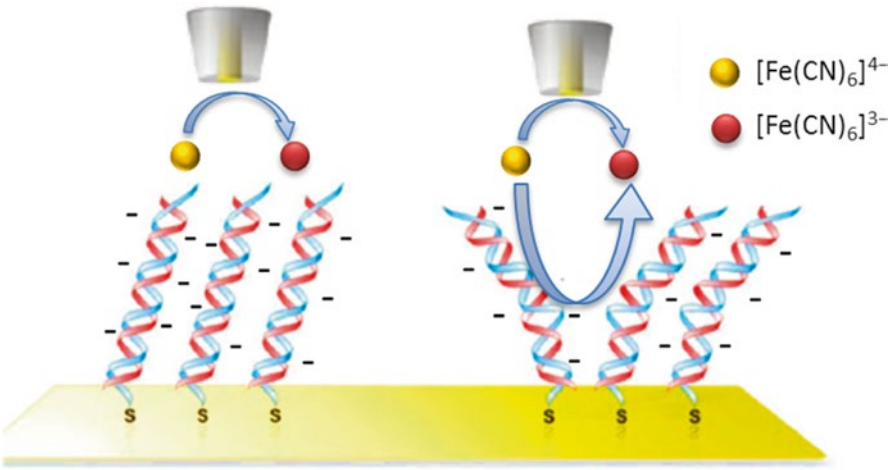

Fig. 6 Scheme depicting the self-assembled ds-DNA on gold surface through Au-S linkage. Well assembled and defect free layer resists the diffusion of the negative redox probe, by physical hindrance as well as negative charge repulsion, to reach the gold surface and get recycled, which ultimately decreases the feedback current on tip. Defects in ds-DNA layer allow the redox mediator to diffuse through the film and give higher feedback current (Adapted from Diakowski P, Kraatz H-B (2011) Towards the electrochemical identification of species. Chem Comm 47:431–1433 with permission from The Royal Society of Chemistry)

Table 2 Apparent electron transfer rate constants determined in the absence and presence of Zn^{2+} (Values extracted from Diakowski P, Kraatz H-B (2009) Detection of single-nucleotide mismatches using scanning electrochemical microscopy. Chem Comm 45:1189–1191)

Strand	k^0/cm s^{-1} (No Zn^{2+})	k^0/cm s^{-1} (Zn^{2+} present)
Fully matched	$3.52 \pm 0.24 \times 10^{-5}$	$7.03 \pm 0.3 \times 10^{-5}$
Bottom mismatch	$6.75 \pm 0.39 \times 10^{-5}$	$2.81 \pm 0.21 \times 10^{-4}$
Top mismatch	$9.98 \pm 0.47 \times 10^{-5}$	$1.26 \pm 0.28 \times 10^{-3}$

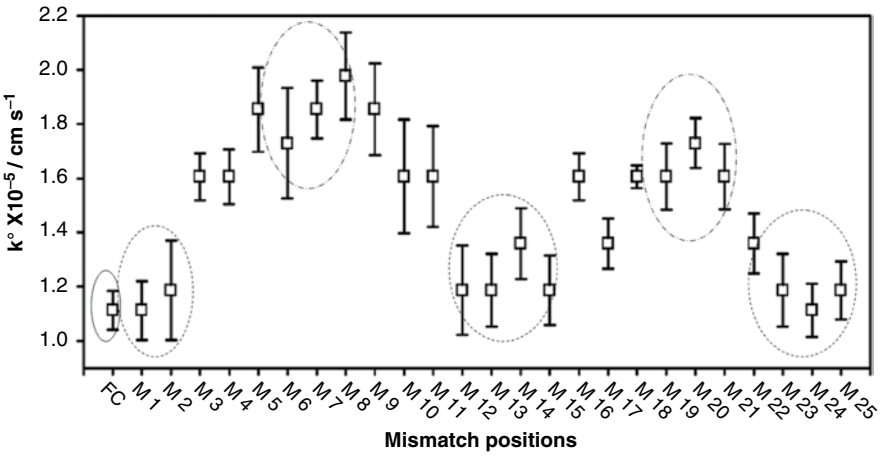

Fig. 7 Apparent rate constant (k^0) with respect to the position of mismatches in the presence of Zn^{2+} ds-DNA film. Error bars were calculated for at least three measurements. *Solid circle* (—) shows fully matched DNA, *dashed circle* (—) represents barely distinguishable single nucleotide mismatch positions and *dash eith dots* (-··-) represnts highly distinguishable mismatch positions (Alam MN, Shamsi MH, Kraatz H-B (2012) Scanning positional variations in single-nucleotide polymorphism of DNA: an electrochemical study. Analyst 137:4220–4225 with permission from The Royal Society of Chemistry)

The heterogeneous electron transfer rates were obtained by finite element method to fit experimental approach curves to theoretical curves. The increase of the electron transfer rate constant (Table 2) in the presence of single-nucleotide mismatches was attributed to better penetration of the redox probe into the film. This is rationalized considering that the presence of a mismatch causes localized distortion in the backbone of the DNA, which ultimately gives rise to defects in the film (Fig. 7). The differences in feedback current and thus rate constants were amplified between matched and mismatched ds-DNA after the addition of Zn^{2+}. The discrimination of positions clearly demonstrates that ds-DNA films with single-nucleotide mismatch at different positions possess different electrochemical properties, presumably with respect to probe penetration. In a separate study based on impedance spectroscopy and SECM, Shamsi and Kraatz found that position of single-nucleotide mismatch is dominant over the type of mismatch.

This means that different mismatch types would give similar electrochemical film properties on surface with the exception of those located in the center of the DNA [40]. Most reported model studies involving mismatches involve the detection of one or two well-defined single-nucleotide mismatches at one or two positions. However, in a real sample, the analyst would be blind of the actual position or nature of the mismatch. Therefore, Kraatz's group decided to map out a single-nucleotide mismatch in all 25 positions of a 25-mer ds-DNA bound to a gold surface [41]. This systematic approach was expected to provide some insight as

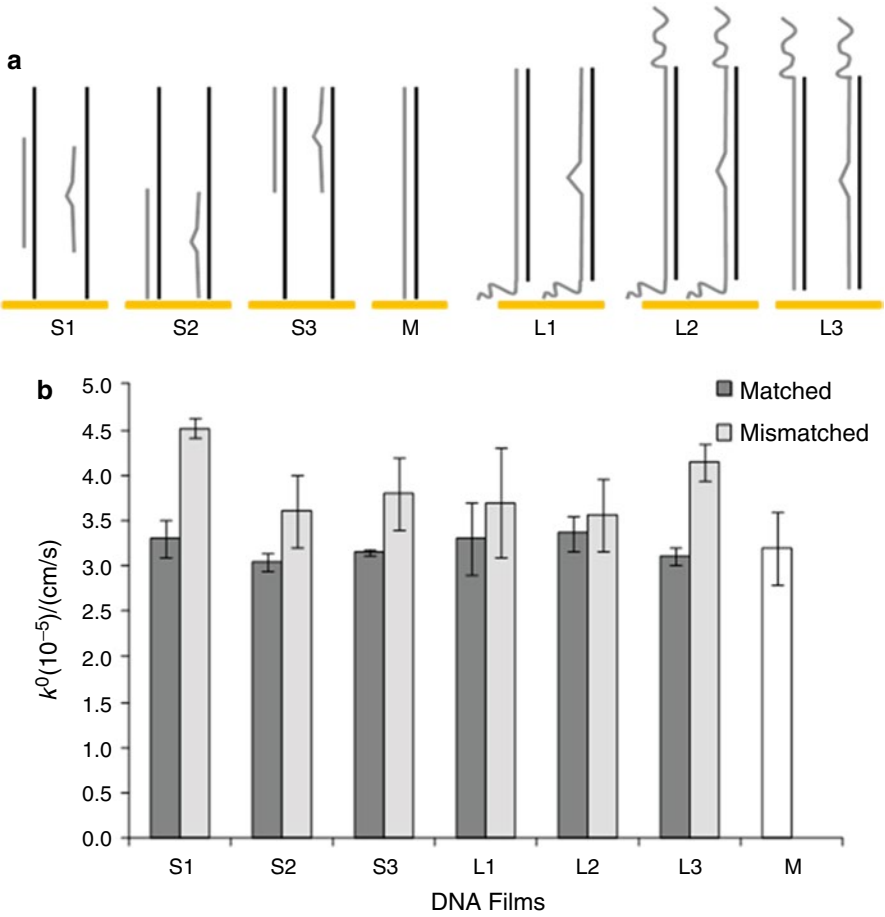

Fig. 8 (**a** and **b**) The ds-DNA films (matched and mismatched) with 25-mer short complementary strands (**S1–S3**), longer complementary strands (**L1–L3**), and exact size 51-mer fully matched (**M**). Estimated kinetic rate (k^0) constants for matched and mismatched duplexes in (**a** and **b**) (Adapted from Shamsi MH, Kraatz H-B (2013) Electrochemical signature of mismatch in overhang DNA films: a scanning electrochemical microscopic study. Analyst 138:3538–3543 with permission from The Royal Society of Chemistry)

to the specificity and sensitivity of this approach. The results showed that ds-DNA films containing single-nucleotide mismatch at the extreme positions along the strand (positions 1, 2, and 23–25) and in the middle of the strand (positions 12–15) show similar electrochemical properties and therefore are barely distinguishable from fully matched ds-DNA films. However, there are positions, which are moderately and highly distinguishable from fully matched duplex as shown in Fig. 8. Moreover, it is suggested that such highly distinguishable and barely distinguishable positions may differ with the length of the duplex. Another interesting issue, which was addressed by the group [42], was related to sample preparation and the inability to control the size of the target sequence. Can mismatches be detected in ds-DNA with unequal lengths of the probe and target strands, causing overhangs at the solution or electrode side of the film? Therefore, in order to study the potential impact of unmatched lengths of probe and target strands, the probe and target strands of unequal size were hybridized in absence and presence of single-nucleotide mismatches along the sequence. As a result of hybridization between unequal lengths of strands, the shorter target sequences formed overhangs in probe strand and longer target sequences formed overhangs in complementary strand. SECM images showed higher feedback current for all mismatched films regardless the length and the type of overhangs (Fig. 9). This is an important result, indicating that SECM is able to distinguish even nonideal

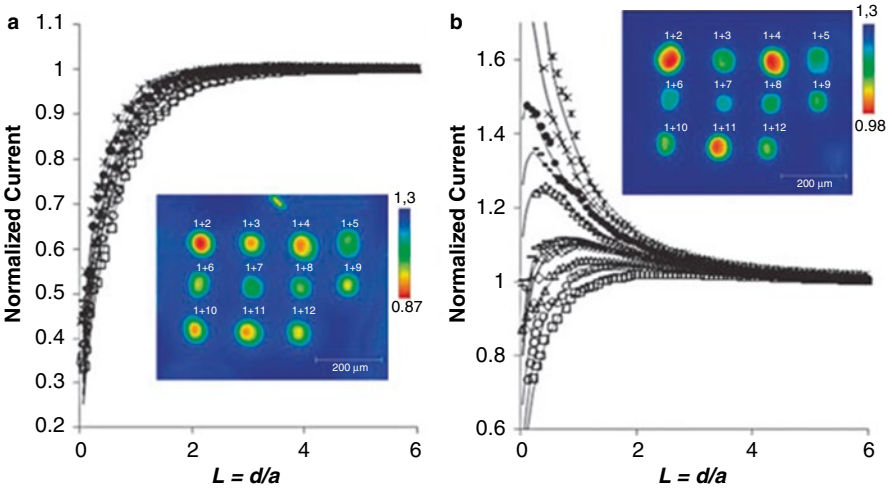

Fig. 9 Normalized approach curves with multiplexed SECM images observed above ds-DNA spots in the absence of Zn^{2+} (**a**) and in the presence of Zn^{2+} (**b**). *Solid lines* represent simulated approach curves. In this study bovine CYTbos1 primer sequence was hybridized with related sequences of animal species of different families which resulted in multiple mismatches along the sequence (Adapted from Diakowski P, Kraatz H-B (2011) Towards the electrochemical identification of species. Chem Comm 47:431–1433 with permission from The Royal Society of Chemistry)

length-mismatched ds-DNA. The kinetic rate constants monitored right above the ds-DNA films showed that hybridization position is critical for mismatch detection in short complementary stands, while mismatches are easily detectable in absence of bottom overhangs in longer complementary strands.

This detailed study on the variation in electrochemical response due to the presence of mismatch in ds-DNA films paved the way to exploit SECM for high-throughput discrimination of animal species. For this purpose, the bovine CYTbos1 primer sequence was hybridized with the related sequences of animal species of different families [13]. A fully matched ds-DNA SECM signature was obtained by hybridization with a bovine complement. Mismatched ds-DNA combinations containing various numbers of mismatches were obtained for pig, chicken, buffalo, deer, quail, and horse. The analysis of a microarray prepared of a range of ds-DNAs of different hybrids shows that different feedback currents are obtained. The magnitude of the feedback current is a function of the position and number of mismatches in the ds-DNA prepared from the CYT1bos1 primer and respective animal strands (Fig. 10). This barcoding approach to DNA testing, by exploiting the mitochondrial CO1 gene, was also effective to detect species from same family of Bovinae, i.e., dairy cattle, North American buffalo, and European buffalo [43]. Essentially, this approach allows the identification of minute quantities of DNA that are admixed to a matrix. This is of course of relevance given the most recent issue with food adulterations of beef and the discovery of nonbeef species in meat meant for human consumption. This clearly brings into focus one of the potential applications of SECM as a bioanalytical tool.

Conclusion

The electrochemical detection of DNA mismatches remains an attractive area of research. Initial studies exploiting voltammetric or amperometric measurements have led to a series of interesting controversies of the electron transfer properties of ds-DNA. More recent impedance spectroscopic studies have been more focused on the colligative properties of the ds-DNA, which has led to the development of label-free mismatch detection with ferri/ferrocyanide as a convenient electroactive probe. It was recognized that resistive differences are responsible for the impedance observations. This brings into focus the recent studies exploiting SECM for monitoring ds-DNA films. SECM allows convenient multiplexing of the measurement, while providing information on the electrochemical properties of the film. In this chapter, the value of SECM for the detection of single-nucleotide mismatches was the focus. Not only is it possible to distinguish any particular mismatch, but it is also possible to obtain information about the positional parameters of the mismatch. A simple application for the identification of animal species is an example for the versatility of SECM for bioanalysis. SECM as a laboratory-based bioanalytical method is undervalued but provides a promising alternative to other assays that make use of

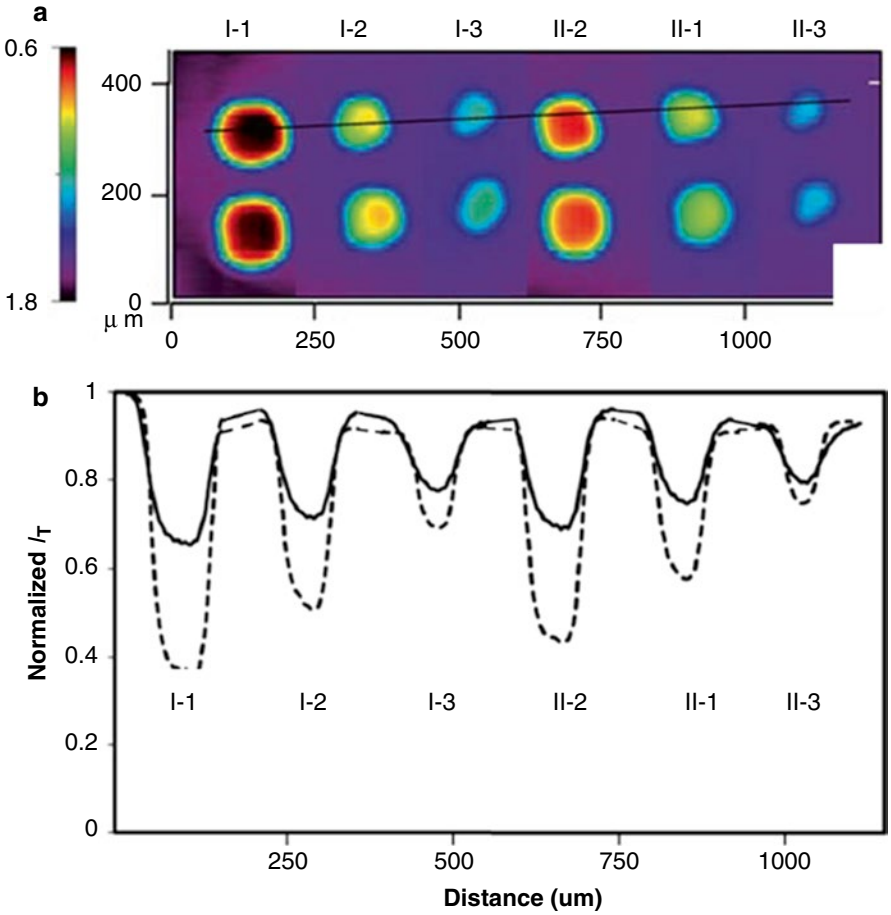

Fig. 10 (**a**) Multiplex detection of Bovine species by SECM images. (**b**) Current profile of DNA duplexes after hybridization of CO1 gene fragments of cow, NA buffalo and European buffalo before Zn^{2+} (*solid line*) and after Zn^{2+} (*dashed line*). I-1 and II-2 are fully matched ds-DNA of cow and North American buffalo respectively. I-2 and I-3 are the mismatched ds-DNA due to cross hybridization between cow CO1 gene with North American buffalo and European buffalo. II-1 and II-3 are the mismatched ds-DNA due to cross hybridization between North American buffalo CO1 gene with cow and European buffalo (Adapted from Shamsi MH, Kraatz H-B (2011) Electrochemical identification of artificial oligonucleotides related to bovine species. Potential for identification of species based on mismatches in the mitochondrial cytochrome C1 oxidase gene. Analyst 136:4724–4731 with permission from The Royal Society of Chemistry)

optical/spectroscopic detection, and one can expect to see significant results in this area over the next few years. Table 3 summarizes some of the key developments in the area of SECM and its application to the study of thin films with particular reference to the study of oligonucleotide films.

Table 3 Selected key references highlighting the development of scanning electrochemical microscopy and its applications

A new approach based on the combination of scanning electrochemical microscopy and surface plasmon resonance imaging (SECM/ SPR-i)	2005	Electroanalysis 17:495–503
Exploring the motional dynamics of end-grafted DNA oligonucleotides by in situ electrochemical atomic force microscopy	2007	J Phys Chem B 111:6051–6058
Scanning electrochemical microscopy for direct imaging of reaction rates	2006	Angew Chemie (Int Ed English) 46:1584–617
Scanning electrochemical microscopy in the 21st century	2007	Phys Chem Chem Phys 9:802–823
Scanning electrochemical microscopy: principles and applications to biophysical systems	2006	Physiol Meas 27:R63–R108
Advances in the application of scanning electrochemical microscopy to bioanalytical systems	2007	Biosens Bioelectron 23:301–318
Recent advances in high resolution scanning electrochemical microscopy of living cells – A review	2013	Analytica Chimica Acta 775:1–13
Measurements within the diffusion layer using a microelectrode probe	1986	Anal Chem 58:844–848
Scanning electrochemical and tunneling ultramicroelectrode microscope for high-resolution examination of electrode surfaces in solution	1986	J Am Chem Soc 108:3838–3839
Scanning electrochemical microscopy. Apparatus and two-dimensional scans of conductive and insulating substrates	1989	Anal Chem 61:1794–1799
Scanning electrochemical microscopy. Theory of the feedback mode	1989	Anal Chem 6:1221–1227
Scanning electrochemical microscopy (SECM): an investigation of the effects of tip geometry on amperometric tip response	1998	J Phys Chem B 102:9946–9951
Towards the electrochemical identification of species	2011	Chem Comm 47:431–1433
Analytical expressions for quantitative scanning electrochemical microscopy (SECM)	2010	ChemPhysChem 1:547–556
Scanning electrochemical microscopy. Effect of defects and structure on electron transfer through self-assembled monolayers	2008	Langmuir 24:2841–2849
Scanning electrochemical microscopy with gold nanotips: the effect of electrode material on electron transfer rates	2009	J Phys Chem C 113:459–464
Effect of base pair A/C and G/T mismatches on the thermal stabilities of DNA oligomers that form B-junctions	1997	Biochemistry 36:11419–11427
Single-base-pair discrimination of terminal mismatches by using oligonucleotide microarrays and neural network analyses	2002	Appl Environ Microbiol 68: 235–244
Electron transfer at self-assembled monolayers measured by scanning electrochemical microscopy	2004	J Am Chem Soc 126:1485–1492

(continued)

Table 3 (continued)

Patterned self-assembled alkanethiolate monolayers on gold. Patterning and imaging by means of scanning electrochemical microscopy	1997	Electroanalysis 9:746–750
Localized electrochemical desorption of gold alkanethiolate monolayers by means of scanning electrochemical microscopy (SECM)	2000	Microchim Acta 133:1–9
Scanning electrochemical microscope observation of defects in a hexadecanethiol monolayer on gold with shear force-based tip–substrate positioning	2006	Langmuir 22:7923–7927
Investigation of carboxylic-functionalized and n-alkanethiol self-assembled monolayers on gold and their application as pH-sensitive probes using scanning electrochemical microscopy	2005	Surf Sci 597:51–64
Studying the binding of Cd^{2+} by ω-mercaptoalkanoic acid self-assembled monolayers by cyclic voltammetry and scanning electrochemical microscopy (SECM)	2005	J Electroanal Chem 581:310–319
Visualization of dna microarrays by scanning electrochemical microscopy (SECM)	2001	Analyst 126:1210–1211
Silver-enhanced imaging of dna hybridization at DNA microarrays with scanning electrochemical microscopy	2002	Langmuir 18:6653–6658
Scanning electrochemical microscopic imaging of surface-confined DNA probes and their hybridization via guanine oxidation	2002	J Electroanal Chem 537:95–102
Scanning electrochemical microscopy imaging of DNA microarrays using methylene blue as a redox-active intercalator	2008	Langmuir 24:5155–5160
Detection of DNA π-Stack lesions using scanning electrochemical microscopy	2009	ECS Transactions 166:55–62
Scanning electrochemical microscopy of DNA monolayers modified with Nile Blue	2008	Langmuir 24:14282–14288
Electron transfer in DNA and in DNA-related biological processes. Electrochemical insights	2008	Chem Rev 108:2622–2645
Label-free electrochemical recognition of DNA hybridization by means of modulation of the feedback current in SECM	2004	Angew Chemie (Int Ed English) 43:3482–3485
Imaging immobilised ssDNA and detecting DNA hybridisation by means of the repelling mode of scanning electrochemical microscopy (SECM)	2004	Biosens Bioelectron 20:925–932
Electrochemical imaging of localized sandwich DNA hybridization using scanning electrochemical microscopy	2007	Anal Chem 79:7206–7213
Optimization of an electrochemical DNA assay by using a 48-electrode array and redox amplification studies by means of scanning electrochemical microscopy	2009	Chem Bio Chem 10:1193–1199
Scanning electrochemical microscopy assay of DNA based on hairpin probe and enzymatic amplification biosensor	2010	Biosens Bioelectron 25:1953–1957

(continued)

Table 3 (continued)

Scanning electrochemical microscopy of genomic DNA microarrays study of adsorption and subsequent interactions	2009	Analyst 134:1302–1308
Scanning electrochemical microscopy. Studies of self-assembled monolayers of DNA in the absence and presence of metal ions	2005	J Phys Chem B 109: 5193–5198
Electrochemical detection of single-nucleotide mismatches using an electrode microarray	2006	Anal Chem 78:6096–6101
Detection of single-nucleotide mismatches using scanning electrochemical microscopy	2009	Chem Comm 45:1189–1191
Probing nucleobase mismatch variations by electrochemical techniques: exploring the effects of position and nature of the single-nucleotide mismatch	2010	Analyst 135:2280–2285
Scanning positional variations in single-nucleotide polymorphism of DNA: an electrochemical study	2012	Analyst 137:4220–4225
Electrochemical signature of mismatch in overhang DNA films: a scanning electrochemical microscopic study	2013	Analyst 138:3538–43
Electrochemical identification of artificial oligonucleotides related to bovine species. Potential for identification of species based on mismatches in the mitochondrial cytochrome C1 oxidase gene	2011	Analyst 136:4724–4731

References

1. Elodie F, Yann D, Pascal M, Thierry L, Sabine S (2005) Micro-imprinting of oligonucleotides and oligonucleotide gradients on gold surfaces: a new approach based on the combination of scanning electrochemical microscopy and surface plasmon resonance imaging (SECM/ SPR-i). Electroanalysis 17:495–503
2. Wang K, Goyer C, Anne A, Demaille C (2007) Exploring the motional dynamics of end-grafted DNA oligonucleotides by in situ electrochemical atomic force microscopy. J Phys Chem B 111:6051–6058
3. Wittstock G, Burchardt M, Pust S, Shen Y, Zhao C (2006) Scanning electrochemical microscopy for direct imaging of reaction rates. Angew Chem Int Ed Engl 46:1584–1617
4. Sun P, Laforge F, Mirkin M (2007) Scanning electrochemical microscopy in the 21st century. Phys Chem Chem Phys 9:802–823
5. Edwards M, Martin S, Whitworth A, Macpherson J, Unwin P (2006) Scanning electrochemical microscopy: principles and applications to biophysical systems. Physiol Meas 27:R63–R108
6. Roberts WS, Lonsdale DJ, Griffiths J, Higson SPJ (2007) Advances in the application of scanning electrochemical microscopy to bioanalytical systems. Biosens Bioelectron 23:301–318
7. Bergner S, Vatsyayan P, Matysik F-M (2013) Recent advances in high resolution scanning electrochemical microscopy of living cells – a review. Anal Chim Acta 775:1–13
8. Engstrom RC, Weber M, Wunder DJ, Burgess R, Winquist S (1986) Measurements within the diffusion layer using a microelectrode probe. Anal Chem 58:844–848
9. Liu H-Y, Fan F-RF, Lin CW, Bard AJ (1986) Scanning electrochemical and tunneling ultramicroelectrode microscope for high-resolution examination of electrode surfaces in solution. J Am Chem Soc 108:3838–3839
10. (a) Kwak J, Bard AJ (1989) Scanning electrochemical microscopy. Apparatus and two-dimensional scans of conductive and insulating substrates. Anal Chem 61:1794–1799; (b)

Kwak J, Bard AJ (1989) Scanning electrochemical microscopy. Theory of the feedback mode. Anal Chem 6:1221–1227
11. Jonathan LA, Guy D (1998) Scanning electrochemical microscopy (SECM): an investigation of the effects of tip geometry on amperometric tip response. J Phys Chem B 102:9946–9951
12. Diakowski P, Kraatz H-B (2011) Towards the electrochemical identification of species. Chem Commun 47:431–1433
13. Lefrou C, Cornut R (2010) Analytical expressions for quantitative scanning electrochemical microscopy (SECM). Chemphyschem 1:547–556
14. Kiani A, Alpuche-Aviles M-A, Eggers PK, Jones M, Gooding JJ, Paddon-Row M-N, Bard AJ (2008) Scanning electrochemical microscopy. 59. Effect of defects and structure on electron transfer through self-assembled monolayers. Langmuir 24:2841–2849
15. Velmurugan J, Sun P, Mirkin MV (2009) Scanning electrochemical microscopy with gold nanotips: the effect of electrode material on electron transfer rates. J Phys Chem C 113: 459–464
16. Otokiti E, Sheardy R (1997) Effect of base pair A/C and G/T mismatches on the thermal stabilities of DNA oligomers that form B-Z junctions. Biochemistry 36:11419–11427
17. Urakawa H, Noble PA, El Fantroussi S, Kelly JJ, Stahl DA (2002) Single-base-pair discrimination of terminal mismatches by using oligonucleotide microarrays and neural network analyses. Appl Environ Microbiol 68:235–244
18. Liu B, Bard AJ, Mirkin MV, Creager SE (2004) Electron transfer at self-assembled monolayers measured by scanning electrochemical microscopy. J Am Chem Soc 126:1485–1492
19. Wittstock G, Hesse R, Schuhmann W (1997) Patterned self-assembled alkanethiolate monolayers on gold. Patterning and imaging by means of scanning electrochemical microscopy. Electroanalysis 9:746–750
20. Wilhelm T, Wittstock G (2000) Localized electrochemical desorption of gold alkanethiolate monolayers by means of scanning electrochemical microscopy (SECM). Microchim Acta 133:1–9
21. Yamada H, Ogata M, Koike T (2006) Scanning electrochemical microscope observation of defects in a hexadecanethiol monolayer on gold with shear force-based tip–substrate positioning. Langmuir 22:7923–7927
22. Boldt F-M, Baltes N, Borgwarth K, Heinze J (2005) Investigation of carboxylic-functionalized and n-alkanethiol self-assembled monolayers on gold and their application as pH-sensitive probes using scanning electrochemical microscopy. Surf Sci 597:51–64
23. Burshtain D, Mandler D (2005) Studying the binding of Cd^{2+} by ω-mercaptoalkanoic acid self assembled monolayers by cyclic voltammetry and scanning electrochemical microscopy (SECM). J Electroanal Chem 581:310–319
24. Kenichi Y, Makoto T, Shigeori T, Kazuhiko U, Hiroki K (2001) Visualization of dna microarrays by scanning electrochemical microscopy (SECM). Analyst 126:1210–1211
25. Jun W, Fayi S, Feimeng Z (2002) Silver-enhanced imaging of dna hybridization at DNA microarrays with scanning electrochemical microscopy. Langmuir 18:6653–6658
26. Wang J, Zhou F (2002) Scanning electrochemical microscopic imaging of surface-confined DNA probes and their hybridization via guanine oxidation. J Electroanal Chem 537:95–102
27. Wain A, Zhou F (2008) Scanning electrochemical microscopy imaging of DNA microarrays using methylene blue as a redox-active intercalator. Langmuir 24:5155–5160
28. Hammonda WJ, Arndta J, Nguyena T, Slowinskaa KU, Jacksonb C, Burgoyneb HA, Hillb MG, Slowinskia K (2009) Detection of DNA π-Stack lesions using scanning electrochemical microscopy. ECS Trans 166:55–62
29. Gorodetsky A, Hammond W, Hill M, Slowinski K, Barton J (2008) Scanning electrochemical microscopy of DNA monolayers modified with Nile Blue. Langmuir 24:14282–14288
30. Boussicault F, Robert M (2008) Electron transfer in DNA and in DNA-related biological processes. Electrochemical insights. Chem Rev 108:2622–2645
31. Turcu F, Schulte A, Hartwich G, Schuhmann W (2004) Label-free electrochemical recognition of DNA hybridization by means of modulation of the feedback current in SECM. Angew Chem Int Ed Engl 43:3482–3485

32. Turcu F, Schulte A, Hartwich G, Schuhmann W (2004) Imaging immobilised ssDNA and detecting DNA hybridisation by means of the repelling mode of scanning electrochemical microscopy (SECM). Biosens Bioelectron 20:925–932
33. Palchetti I, Laschi S, Marrazza G, Mascini M (2007) Electrochemical imaging of localized sandwich DNA hybridization using scanning electrochemical microscopy. Anal Chem 79: 7206–7213
34. Neugebauer S, Zimdars A, Liepold P, Gebala M, Schuhmann W, Hartwich G (2009) Optimization of an electrochemical DNA assay by using a 48-electrode array and redox amplification studies by means of scanning electrochemical microscopy. Chem Bio Chem 10: 1193–1199
35. Zhang Z, Zhou J, Tang A, Wu Z, Shen G, Yu R (2010) Scanning electrochemical microscopy assay of DNA based on hairpin probe and enzymatic amplification biosensor. Biosens Bioelectron 25:1953–1957
36. Roberts W, Davis F, Higson S (2009) Scanning electrochemical microscopy of genomic DNA microarrays study of adsorption and subsequent interactions. Analyst 134:1302–1308
37. Liu B, Bard A, Li C-Z, Kraatz H-B (2005) Scanning electrochemical microscopy. 51. Studies of self-assembled monolayers of DNA in the absence and presence of metal ions. J Phys Chem B 109:5193–5198
38. Li X, Lee JS, Kraatz H-B (2006) Electrochemical detection of single-nucleotide mismatches using an electrode microarray. Anal Chem 78:6096–6101
39. Diakowski P, Kraatz H-B (2009) Detection of single-nucleotide mismatches using scanning electrochemical microscopy. Chem Commun 45:1189–1191
40. Shamsi MH, Kraatz H-B (2010) Probing nucleobase mismatch variations by electrochemical techniques: exploring the effects of position and nature of the single-nucleotide mismatch. Analyst 135:2280–2285
41. Alam MN, Shamsi MH, Kraatz H-B (2012) Scanning positional variations in single-nucleotide polymorphism of DNA: an electrochemical study. Analyst 137:4220–4225
42. Shamsi MH, Kraatz H-B (2013) Electrochemical signature of mismatch in overhang DNA films: a scanning electrochemical microscopic study. Analyst 138:3538–3543
43. Shamsi MH, Kraatz H-B (2011) Electrochemical identification of artificial oligonucleotides related to bovine species. Potential for identification of species based on mismatches in the mitochondrial cytochrome C1 oxidase gene. Analyst 136:4724–4731